 doi:10.20944/preprints202207.0440.v1

Article

The IASI Water Deficit Index to Monitor the Vegetation Stress and the Early Drying in Summer Because of Heatwaves: an Application to Southern Italy

Guido Masiello[1*], Francesco Ripullone[2], Italia De Feis[3], Francesco Ripullone[3], Angelo Rita[4], Luigi Saulino[4], Pamela Pasquariello[1], Angela Cersosimo[1] , Sara Venafra[1*] and Carmine Serio[1]

[1] Scuola di Ingegneria, Università della Basilicata, 85100 Potenza, I
[3] Scuola di Scienze Agrarie, Forestali, Alimentari ed Ambientali, Università della Basilicata, 85100 Potenza, I
[2] IAC-CNR, Napoli, I
[4] Dipartimento di Agraria, Università di Napoli Federico II, 80055 Portici (NA), I
* Correspondence: guido.masiello@unibas.it; sara.venafra@unibas.it

Abstract: The boreal Hemisphere has been experiencing increasing extreme hot and dry conditions over the past few decades, consistent with anthropogenic climate change expectations. The continental extension of the phenomenon calls for tools and techniques capable of monitoring the global to regional scales. In this context, the satellite is the only system that can satisfy the need for global coverage. The main objective we have addressed in the present paper is the capability of infrared satellite observations helping to monitor the vegetation stress due to increasing drought and heatwaves in summer. We have designed and implemented a new water deficit index (*wdi*) that exploits satellite observations in the infrared to retrieve humidity, air temperature, and surface temperature simultaneously. These three parameters are combined to provide the water deficit index. The index has been developed based on the Infrared Atmospheric Sounder Interferometer or IASI, which covers the infrared spectral range 645 to 2760 cm^{-1} with a sampling of 0.25 cm^{-1}. The index has been used to study the 2017 heatwave, which hit Continental Europe from May to October. In particular, we have examined Southern Italy, where Mediterranean forests suffer from climate change. We have computed the index's time series and show that it can be used to indicate the atmospheric background conditions associated with meteorological drought. We have also found a good agreement with soil moisture, which suggests that the persistence of anomalously high water deficit index was an essential driver of the rapid development and evolution of the exceptionally severe 2017 droughts.

Keywords: climate change; drought; water deficit index; infrared observations; satellite; remote sensing; surface temperature; air temperature; humidity; dew point temperature

1. Introduction

The ECMWF or European Centre for Medium-Range Weather Forecasts has determined that winter 2020 was the hottest winter season ever recorded in Europe (e.g., see. https://climate.copernicus.eu/boreal-winter-season-1920-was-far-warmest-winter-season-ever-recorded-europe-0). An event that is now repeated year after year. Furthermore, the Copernicus Climate Change Service (C3S) dataset (e.g., see https://climate.copernicus.eu/esotc/2021/globe-in-2021) shows that the last seven years have been the warmest on record, and the 2021 varies from fifth to seventh warmest.

The present analysis is most relevant to temperate regions and the Mediterranean vegetation. In this respect, [1] discussed the risks of climate change altering sustainable development in the Mediterranean area. Furthermore, in [2], it has been shown that long-lasting droughts induce dieback phenomena in temperate and Mediterranean climate regions, an issue that has also been addressed in [3], which analysed the effect of the 2017 summer heatwave in Europe.

Preprints (www.preprints.org) | NOT PEER-REVIEWED | Posted: 29 July 2022 doi:10.20944/preprints202207.0440.v1

The continental extension of the phenomenon calls for tools and techniques capable of monitoring the global to regional scales. In this context, the satellite is the only system that can satisfy the need for global coverage. The main objective we have addressed in the present paper is the capability of infrared satellite observations helping to monitor early drying in summer because of drought and heatwaves.

Vegetation stress due to water deficit is widespread in many countries due to climate change (e.g., see [2, 3]). Drought is an extreme natural event typical of semi-arid areas and much of the Mediterranean, especially the part of the middle latitudes. The lack of rain for long periods increases the danger and risk of forest fires in areas rich in vegetation and wooded areas. Furthermore, in semi-arid regions, the lack of rain causes water stress. Therefore, the deficit of rainfall and/or water, in general, requires specific actions to monitor and detect the drought condition to mitigate its adverse impacts on human health, wildlife and plant communities.

Water deficit can be estimated using (1) meteorological data; and (2) remote sensing.

The present study aims at a synergetic use of these two different methods to develop new vegetation dryness indices based on the surface temperature, complemented with atmospheric temperature and water vapor mixing ratio or parameters depending on it, such as dew point temperature.

In general, the problem has been studied through the use of indexes such as VDI or Vegetation Dryness Index (or VDI), the TVDI or Temperature Vegetation Dryness Index (TVDI), and the improved TVDI or iTVDI (among many others, see [4-6]). These indices are based on the NDVI (normalized differential vegetation index), the surface temperature, T_s, and the air temperature close to the surface, or T_a. The problem with NDVI is that it is a greenness index and cannot distinguish bare soil from senescent vegetation (e.g., see [7]). In addition, neither T_s nor T_a are directly linked with soil moisture. It should be observed that the use of T_s-NDVI relationships has been long investigated for application to drought assessment, and it has been found to produce inconsistent results in some specific situations (e.g., [8]).

Conversely, we propose to follow the strategy of using surface temperature (T_s), and the dew point temperature (T_d), which are more closely related to surface type and coverage, and soil moisture. The water deficit index is then defined according to the linear difference T_s-T_d.

The water deficit index is meant for analysis at the regional scale; therefore, we need the use of satellite data to ensure the correct spatial coverage and time sampling. Toward this objective, we have used the hyper-spectral satellite infrared sounder (Infrared Atmospheric Sounder Interfemoter or IASI, e.g., [9]) flying on board the European Meteorological Platforms (MetOp). By adequately exploiting IASI observations, we can simultaneously retrieve T_s and T_w, which limit problems of time-space colocation.

We acknowledge that water deficit indices are quite common in-field analyses related to horticulture, e.g., irrigation management, evaluation of crop water stress, and so on (e.g., see [10] and references therein). However, in these cases, we are normally in the presence of temporary water deficit anomalies. In contrast, our approach is meant to account for the background atmospheric humidity and temperature related to drought onset and development (e.g., see [11]). For satellite-based analysis, a similar approach has been proposed in [12], using the concept of vapour pressure deficit (VPD), the difference between the saturation and actual vapour pressure for a given time. In contrast, our approach uses T_d, which is related to VPD, and T_s to build the difference T_s-T_d, allowing us to separate the hot-dry from humid-warm weather conditions better.

2. Materials and Methods

2.1. Material and data

The retrieval from space observations of T_s, and T_d have been performed using the Infrared Atmospheric Sounder Interferometer or IASI [9]. IASI has been developed in France by CNES and is flying on board the Metop platforms, which are satellites of the

Preprints (www.preprints.org) | NOT PEER-REVIEWED | Posted: 29 July 2022 doi:10.20944/preprints202207.0440.v1

EUMETSAT European Polar System (EPS). IASI has been primarily designed as a meteorological mission; hence its main objective is to provide relevant information on temperature and water vapour profiles. The spectral coverage of the instrument extends from 645 to 2760 cm^{-1}; its sampling interval is $\Delta\sigma$=0.25 cm^{-1}, therefore the instrument provides 8461 or channels, i.e., spectral observations for every spectrum.

IASI is a cross-track scanner with 30 adjacent Field of Regard (FOR) per scan, spanning an angular range of ±48.33° on either side of the nadir. The FOR viewing geometry consists of a 2×2 matrix of IFOVs or Instantaneous Fields of Views. In turn, the single IFOV has a diameter of 0.8394°, corresponding to a ground resolution of 12 km per nadir for a satellite altitude of 819 km. The 2×2 IFOV matrix is centered on the viewing direction. At nadir, a FOR of 4 IASI IFOVs (or pixels) covers the ground a square area of ≈50×50 km^2. The corresponding FORs (among the 30 views) are ±1.67° on each side from the nadir direction. The reader interested to further details about IASI and its mission objectives is referred to [9].

Figure 1 shows the target area we have focused on in the paper. The site corresponds to Southern Italy, with the Apennine chains covered by forest, as exemplified by the 2018 Corine land cover (https://land.copernicus.eu/pan-european/corine-land-cover). The two black spots identify two forest areas, where towers to measure gaseous exchange between the canopy and the atmosphere and phenological parameters have been deployed since 2002.

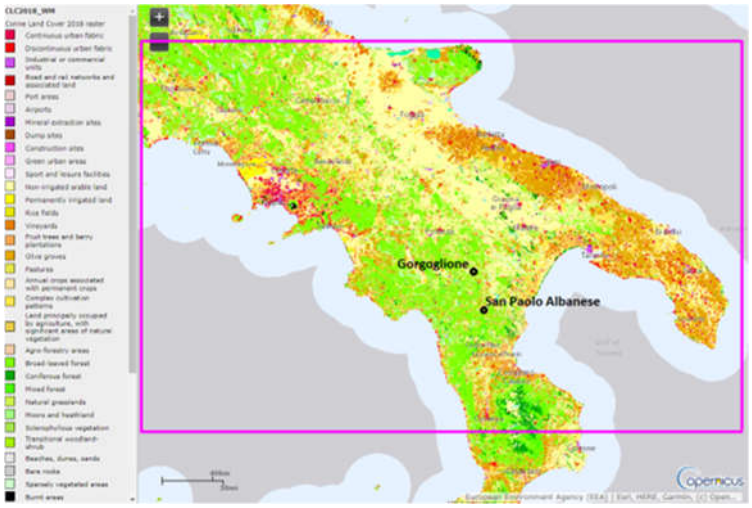

Figure 1. Target region for which IASI data have been selected for the present analysis. The figure also shows the Corine land cover for 2018 to help identify forest regions, which are primarily of interest for this study.

The two locations circled in the maps of Fig. 1 correspond to the forest stands of San Paolo Albanese (40.02° N, 16.34° E, 950–1050 m a.s.l.) and Gorgoglione (40.40° N, 16.14° E, 800–850 m a.s.l.), which are suffering from long-lasting droughts-induced tree mortality (e.g., [2]). In the San Paolo Albanese site, the vegetation is formed by a pure high forest of *Q. frainetto* Ten. for a stand density of 348 trees ha^{-1}. As far as the most affected stands are concerned, recent studies observed that more than 50% of the mature specimens showed symptoms of death, while about 15% died recently [13]. On the other hand, the Gorgoglione woodland is a high-mixed forest, with an average density of about 600 stems ha^{-1}. The vegetation is dominated by *Quercus cerris L.* (71%), followed by *Quercus pubescens L.* (25%) and, with lower density (4%), other species of deciduous trees.

The two main studied tree species showed recent drought-induced decline symptoms since the early 2000s (shoot dieback, summer leaf loss, withering, growth decline, and high mortality). According to local reports about the study area, the yearly oak mortality interested ca. 450 ha. The incidence of the decline syndrome raised mortality from 5 to 10% from 2002 to 2004 [14].

Preprints (www.preprints.org) | NOT PEER-REVIEWED | Posted: 29 July 2022 doi:10.20944/preprints202207.0440.v1

IASI soundings have been acquired for the whole year 2017 when an intense heat wave hit Europe and the Mediterranean area in summer (e.g., see [3]. For comparison, we have also acquired IASI data for 2020 and 2021.

For a proper comparison with our IASI T_s-T_d index, for the same target area and the year 2017, the Copernicus Global Land Service (https://land.copernicus.eu/global/products) has been used to get data about the surface soil moisture (ssm) and the leaf area index (LAI).

The surface soil moisture is derived by observing the band C SAR onboard the satellite Sentinel-1. Data are provided with timeliness of one day at the spatial resolution of ~1 km. For details about the ssm product, we refer the interested reader to [15].

The leaf area index is globally estimated at a spatial resolution of about 300 m through a neural net approach. The input to the net is obtained from instantaneous Top-of-Canopy reflectances from the OLCI (Ocean and Land Colour Imager) instrument onboard the Sentinel-3 satellite or daily Top-of-Aerosol reflectances from the PROBA-V satellite. We refer the interested reader to [16] for further details about the LAI data.

Finally, data about ecophysiological responses of trees for the forest stands of San Paolo Albanese and Gorgoglione have been measured, and used in the present analysis, during two field campaigns performed in July-September 2020 and 2021.

2.2. Methods

IASI will add unique capabilities to the present study because we can simultaneously retrieve T_s, T_d (e.g., [17-20]) from this instrument. To this end, we have developed two retrieval prototypes: one for simultaneous inversion of infrared observations (level 2 or L2 prototype) and the second for remapping L2 products on a regular grid (L3 prototype). The L2 prototype consists of an Optimal Estimation scheme (e.g., [21]), which simultaneously inverts the *full* IASI spectrum to retrieve the state vector, which is made up of the surface emissivity, ε, the surface temperature, T_s, the atmospheric profiles of temperature (T), water vapour (Q), ozone (O), HDO (D), carbonyl sulfide or OCS and scalar scaling factors for the column amount of CO_2, CO, N_2O, CH_4, SO_2, HNO_3, NH_3, and CF_4. However, the parameters relevant to the present analysis are T_s, and the atmospheric profiles for T and Q. Our L2 prototype for IASI has been variously validated as far as the surface parameters and T and Q profiles are concerned. Validation for surface parameters can be found, e.g., in [22, 23], whereas for T and Q in [19, 24].

We are interested in geophysical parameters close to the surface therefore from the profiles of T and Q, we consider only the elements, which correspond to the lowermost atmospheric layer, say T_1 (in units of K) and Q_1 (in units of gr/Kg). The corresponding layer pressure will be denoted with P_1 (in units of hPa). The computation of the dew point temperature, T_d involves the calculation of the actual and saturation water vapour pressures. These will be referred to as P_w, and P_{ws}, respectively. From Q_1 we can compute P_w according to

$$P_w = 10^{-3} P_1 Q_1 \frac{R_w}{R_{air}} \qquad (1)$$

with P_w in hPa and where $R_w = 461.5$ J K^{-1} Kg^{-1} and $R_{air} = 286.9$ J K^{-1}Kg^{-1} are the specific gas constant of water vapour and air, respectively. According to [25], P_{ws} is computed with the formula,

$$P_{ws} = \frac{10^{-2} \times \exp\left(34.494 - \frac{4924.99}{t_1 + 237.1}\right)}{(t_1 + 105)^{1.57}} \qquad (2)$$

with $t_1 = T_1 - 273.15$ (temperature in degrees Celsius) and P_{ws} in hPa. Equation (2) is valid for $t_1 > 0$ (vapor pressure of water). From (1) and (2), we obtain the fractional relative humidity,

$$rh = \frac{P_w}{P_{ws}} \qquad (3)$$

Preprints (www.preprints.org) | NOT PEER-REVIEWED | Posted: 29 July 2022 doi:10.20944/preprints202207.0440.v1

In passing, from (1) and (2), we can also compute the Vapour Pressure Deficit, or $VPD = P_{ws} - P_w$. Finally, the dew point temperature, T_d can be calculated by using the well-known Magnus formula (e.g., [26])

$$t_d = \frac{cx}{b-x},\ x = \ln(rh) + \frac{bt_1}{c+t_1} \quad (4)$$

Where t_d is in degrees Celsius (we will use T_d when referring to degrees Kelvin units), and, $b = 17.62$ (dimensionless), $c = 243.12$ C. Finally, the IASI-based water deficit index or wdi, is defined according to

$$wdi = T_s - T_d = t_s - t_d \quad (5)$$

If needed, Eq. (5) stresses that the index can be computed indifferently with both temperatures in K or C degrees.

The parameter wdi, when referring to a surface covered by vegetation or crops, can help to understand the water stress or deficit during long-lasting droughts or heatwaves. This is because vegetation releases water into the atmosphere through transpiration. The process involves the vaporization of liquid water in plant tissues and the consequent release of vapour into the atmosphere (for example, see [27])). Like direct evaporation, transpiration depends on the amount of energy available, that is, solar radiation in our case, the wind, and the vapour pressure gradient at the surface-atmosphere interface. Consequently, solar radiation, air temperature and humidity, and wind velocity must be considered when evaluating and assessing a satellite-based index to quantify water deficit.

In Eq. (5) the role of energy supply is modeled with T_s. The sun's radiation will cause a rapid increase in the surface temperature of the land. On the other hand, T_d will take into account both air temperature and air humidity. The effect of wind is more difficult to introduce. However, drought and heatwave conditions minimize the spatial gradient and wind intensity. The air subsidence and low intense pressure gradients characterize meteorological conditions that favor summer heatwaves.

It is also important to stress that evaporation and transpiration co-occur, and there is no easy way of distinguishing between the two processes. For this reason, we mention evapotranspiration when referring to the water exchange between vegetation and the air. In addition to water availability in the topsoil, evaporation from the cultivated terrain depends, as already mentioned, on the amount of impinging solar radiation. The solar energy at the surface decreases during crop growth because its foliage or canopy shadows the area below from the sun's rays as the crop develops. Therefore, water is predominately lost by soil evaporation when the crop is small or the leaves are not well developed. However, transpiration becomes the main process once the crop and leaves are well developed and completely cover the soil.

With this in mind, the parameter wdi can help to identify different regimes of water deficit,

1. $wdi \gg 0$; this regime characterizes very hot and dry conditions that favour evapotranspiration. Furthermore, in this regime, the evapotranspiration increases almost linearly with the wind speed (e.g., [27]).
2. $wdi \geq 0$; this regime characterizes warm and humid conditions when the air is already close to saturation; therefore, less additional water can be stored, so the evapotranspiration rate is even lower than for arid land.
3. $wdi \leq 0$; this is the regime $T_s < T_d$ and therefore, the vapour condenses in liquid water at the surface.

Before ending this section, we also note that when wdi is determined by L2 satellite observations, as in our case, we get data that are sparse and not homogeneously covering a given spatial region. Therefore, to better compare with other data sources and perform a correct collocation with stations at the ground, we will use a resampling tool, which can

Preprints (www.preprints.org) | NOT PEER-REVIEWED | Posted: 29 July 2022 doi:10.20944/preprints202207.0440.v1

remap wdi data to a regular grid. To this end, we use the tool developed in [28]. The technique is based on a 2-Dimensional (2D) Optimal Interpolation (OI) scheme and is derived from the broad class of Kalman filter or Bayesian estimation theory. For further details, we refer the interested reader to [28].

The steps involved in the mapping on a regular grid are exemplified in Fig. 2 using the IASI retrieval for wdi for July 2017. Figure 2a and 2d show the IASI data points for T_s, and T_d, which are accumulated considering all the IASI overpasses for July 2017. As said before, the IASI scan pattern is made up of footprints with circular diameters of about 12 km at nadir, and the scanning lines are 50 km apart along the flight direction of the satellite. The IASI scan pattern over the target area for a single overpass is shown in Fig. 3 for the benefit of the reader. Comparing Fig. 3 with Fig. 2a,2c, it is seen that after one month, the IASI clear sky footprints (we stress that we use only observations in a clear sky) are densely distributed over the area much more than the single IASI scan pattern overpass. The monthly ensemble of satellite overpasses improves the sampling of spatial data and, therefore, allows, for example, a better comparison with in situ observations. We use the ensemble of multiple observations to build a map with a better spatial sampling. Towards this objective, we use the 2D OI method, which remaps the data into a grid with a finer mesh than the original data.

The final mesh we use has a spatial sampling of 0.05°× 0.05°. Another important aspect of OI remapping is the use of background fields. This field is built up by using the time and space co-located ECMWF (European Centre for Medium-Range Weather Forecasts) analysis. The ECMWF fields are available on a grid-mesh of 0.5°×0.5°, and the values for T_s, and T_d, interpolated at the IASI L2 products, uneven grid-mesh are exemplified in Fig. 2b,2d, respectively. Based on the coarse ECMWF background, the un-gridded L2 IASI observations and the 2-D OI yields the results shown in Fig. 4, that is, the wdi map at a sampling of 0.05°× 0.05°. In this process, we lose temporal resolution, but we get a map with an improved spatial sampling. We also stress that before remapping, we first build up the difference $T_s - T_d$ from the IASI retrievals and the ECMWF background, then we apply the 2-D OI to this temperature difference.

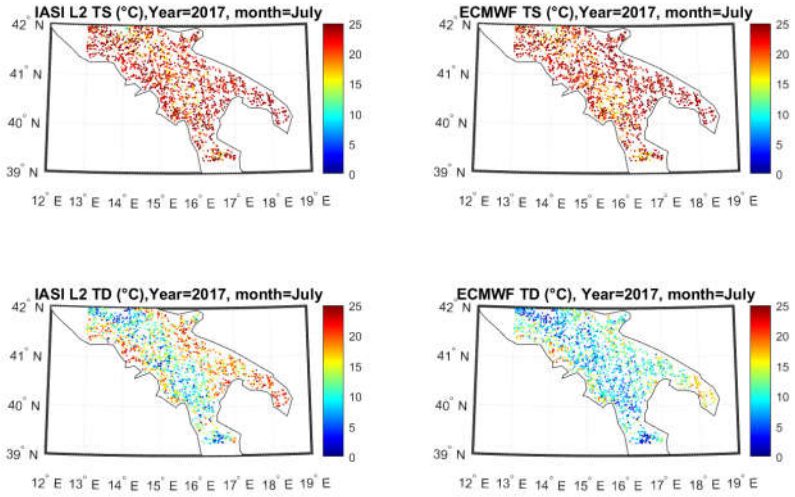

Figure 2. July 2017. IASI L2 retrievals for T_s, (panel a) and T_d (panel c) over the target area. The figure also shows the ECMWF background field interpolated at the IASI retrieval coordinates; panel c refers to T_s, whereas panel d) to T_d.

Preprints (www.preprints.org) | NOT PEER-REVIEWED | Posted: 29 July 2022 doi:10.20944/preprints202207.0440.v1

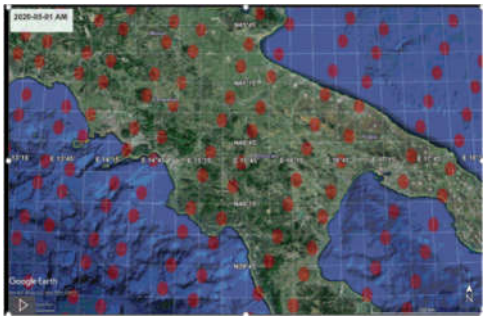

Figure 3. Target region showing the IASI footprint scan pattern (red ovals) for one single overpass. The IASI morning overpass for May, the first of 2020 is shown in the figure. .

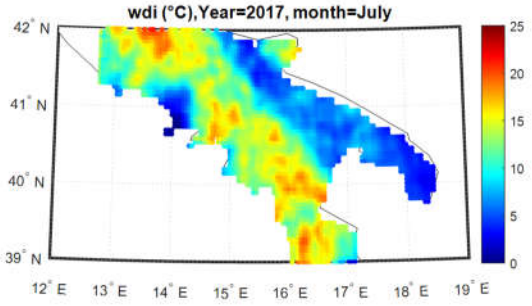

Figure 4. Level 3 map at a grid step of 0.05 degrees for the index *wdi* obtained from the source data shown in Fig. 2. The map is exemplified for July 2017.

3. Results

The rise and fall of the exceptionally hot and drought summer are well captured by the monthly time series of ***wdi*** maps shown in Fig. 5. Of particular interest for us is the Apennine chain, which is covered by broad-leaved, deciduous forests. If we compare Fig. 5 to the land cover map shown in Fig. 1, we see that the ***wdi*** closely follows the forested area in the summer season. In July and August 2017, the index was above ~10 °C in the regions covered by forests, which shows that the vegetation ecosystem was suffering from a water deficit.

To understand the sensitivity of the index to heat waves, we have compared the ***wdi*** parameter over three consecutive years, 2017, 2020, and 2021, for July. We know that July 2020 has been relatively wetter with respect to 2017 and 2021. The comparison is shown in Fig. 6, and we see that ***wdi*** is able to see that the year 2020 has been less warm than the other two. This situation is also reflected in the soil moisture maps shown for the same target area and year and month. When we focus on the forested area, especially in the Southern part of the map, we see that the soil moisture follows the same spatial-time evolution as ***wdi*** and, in particular, the soil moisture is lower in 2017 and 2021 than in 2020. This is a significant result because it shows that the ***wdi*** is capable of capturing processes at the interface surface-atmosphere. A large ***wdi*** means a high rate of evapotranspiration; that is, trees lose water in the atmosphere. The fact that the soil moisture is getting lower means that the vegetation can catch less water from the surface. In conclusion, this is why we think that ***wdi*** can monitor the situation of water deficit during intense heatwaves.

Preprints (www.preprints.org) | NOT PEER-REVIEWED | Posted: 29 July 2022 doi:10.20944/preprints202207.0440.v1

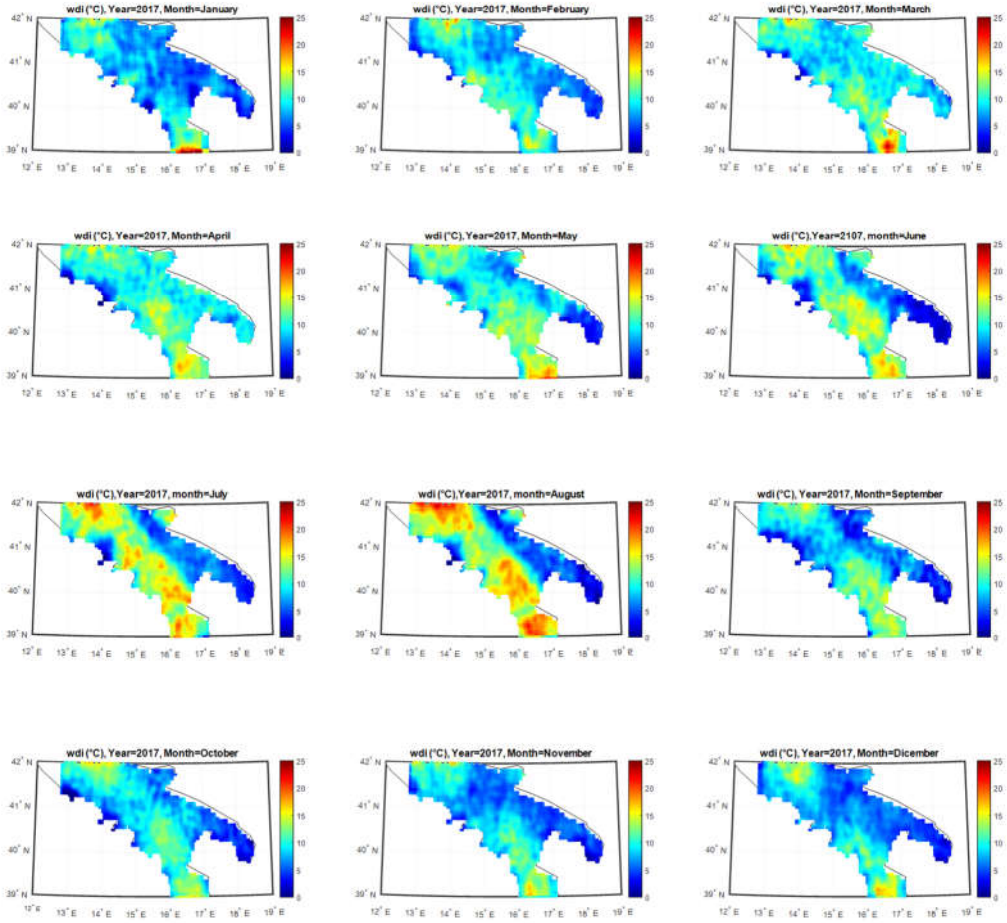

Figure 5. Level 3 map at a grid step of 0.05 degrees for the index *wdi* for 2017.

A further comparison with other parameters which are felt to be sensitive to vegetation stress is shown in Fig. 7 and Fig. 8. Concerning the 2017 heatwave, Fig. 7 compares the surface soil moisture (*ssm*) against *wdi* for the period June to August. It is seen that while *wdi* tends to increase with time, *ssm* does the opposite. The Leaf Area Index (LAI) is another crucial parameter check for vegetation stress. In effect, under the action of an intense heat wave, trees tend to lose leaves to protect from the fierce evapotranspiration. Trees use this mechanism, e.g., in winter, when the light is not enough to sustain the photosynthesis activity. The comparison with *LAI* is shown in Fig. 8, and we see that consistently with the increasing *wdi* behaviour, *LAI* is decreasing from June to July. In normal situations, the *LAI* decrease is not expected in the summer when there is more significant availability of light to sustain photosynthesis. As said before, the decrease is a sign of water deficit because of the intense heatwave.

Preprints (www.preprints.org) | NOT PEER-REVIEWED | Posted: 29 July 2022 doi:10.20944/preprints202207.0440.v1

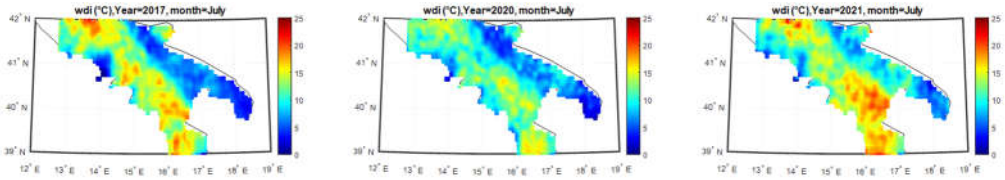

Figure 6. Exemplifying the *wdi* evolution through the years. From left to right (clockwise): July 2017, 2020,2021.

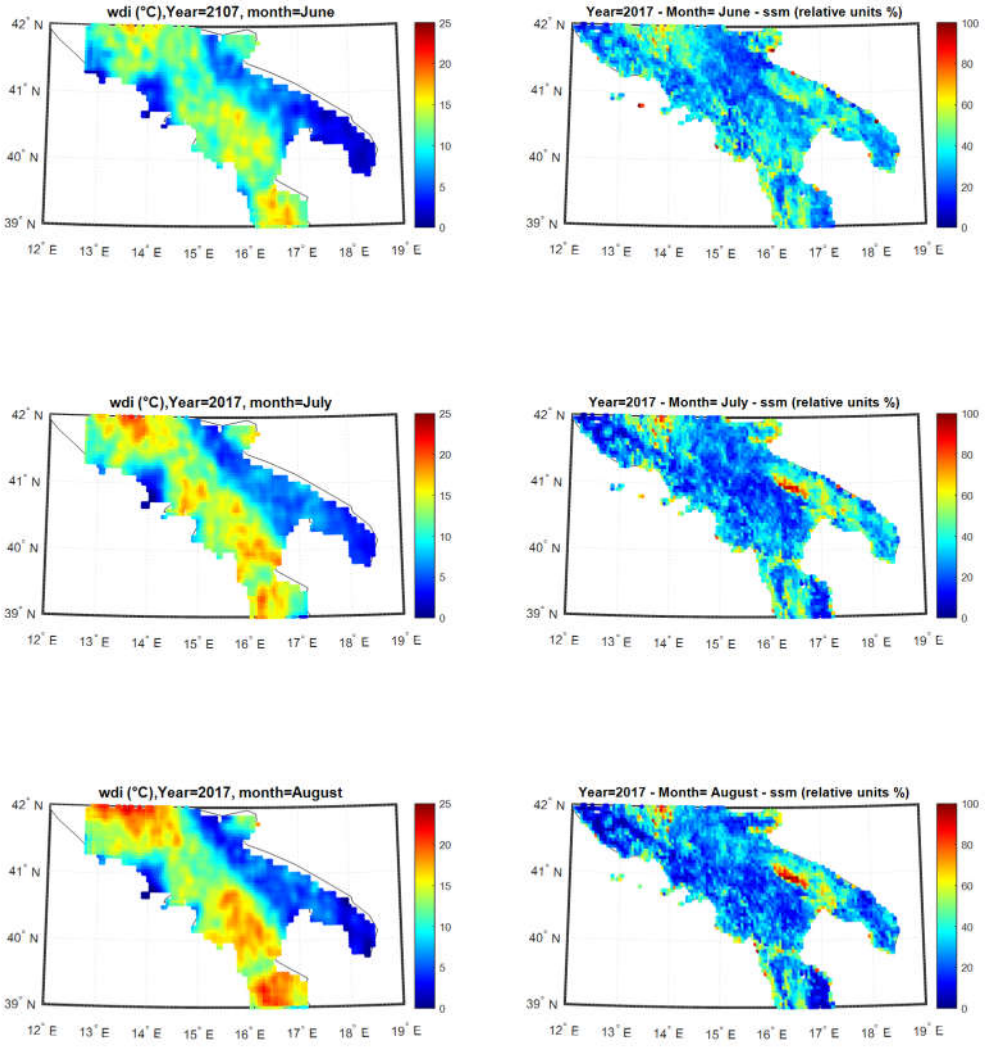

Figure 7. Comparison of *ssm* vs. *wdi* for the period June to August in 2017. Top to bottom, June to August.

Preprints (www.preprints.org) | NOT PEER-REVIEWED | Posted: 29 July 2022 doi:10.20944/preprints202207.0440.v1

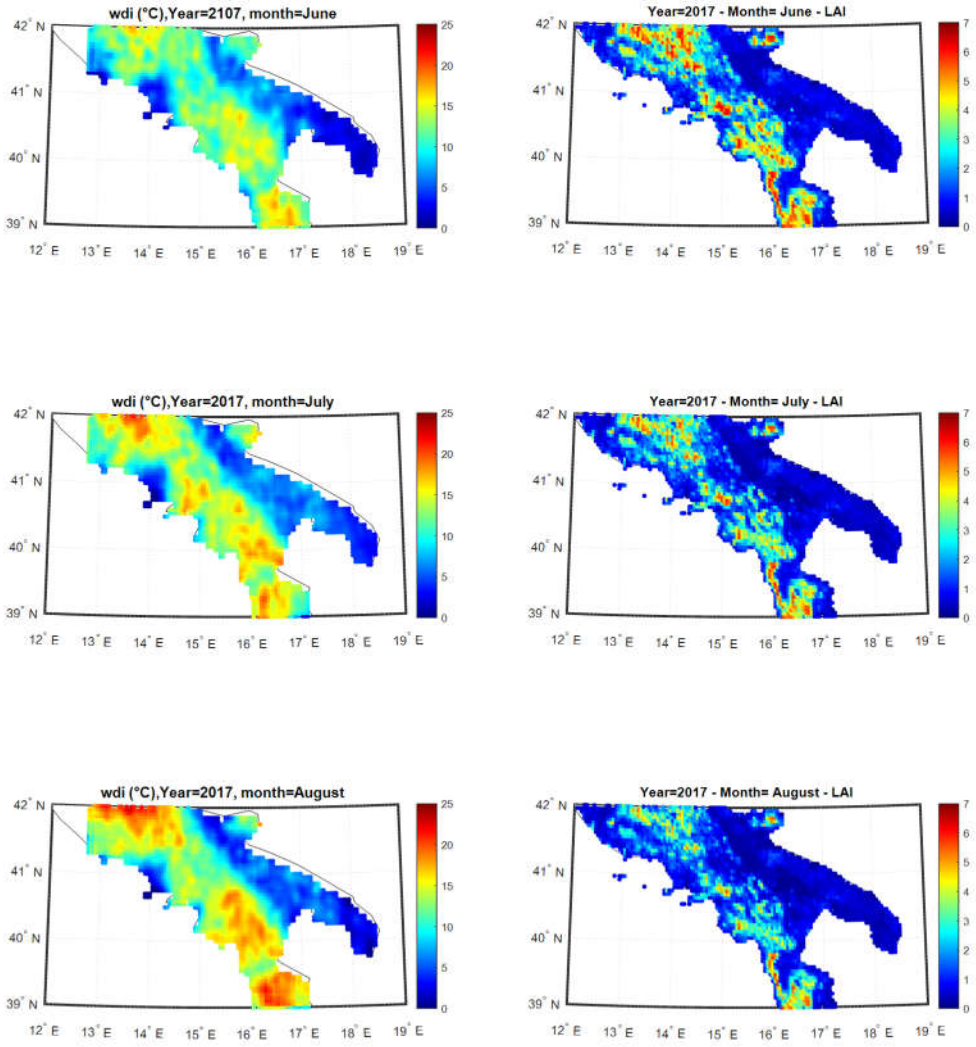

Figure 8. Comparison of *LAI* (m^2/m^2) vs. *wdi* for the period June to August in 2017. Top to bottom, June to August.

We have also checked that the good consistency among *ssm*, *LAI*, and *wdi* also persists at the local scale. In fact, for the two stations of S. Paolo Albanese and Gorgoglione, shown in Fig. 1, we have computed the monthly time series of *ssm* and *wdi* for 2017. The time series are shown in Fig. 9, and we see that starting from May until September, *wdi* goes up, whereas *ssm* have the opposite behaviour. Again, this is an important result because it shows that the *wdi* is capturing a water deficit condition for the vegetation, especially in the area where we know that are declining trees.

A most striking agreement is seen when comparing in situ observations for the flux exchange of CO_2 and H_2O from trees to the *wdi* parameter. In the summer of 2020 and 2021, CO_2 exchange measurements were performed at leaf scale both on declining and non-declining *Q. frainetto* trees growing at the S. Paolo Albanese study site. In each tree, net photosynthesis rate (An, $\mu molCO_2\ m^{-2}\ s^{-1}$), stomatal conductance (gsw, $mmolH_2O\ m^{-2}\ s^{-1}$), and intrinsic water use efficiency (WUEi, $\mu molCO_2\ mmol^{-1}\ H_2O$) were measured by using portable Photosynthesis System LiCOR 6400xt equipped with the 6400-40 Leaf Chamber Fluorometer.

In the summers of 2020 and 2021, the ecophysiological response of *Q. frainetto* trees exhibiting decline and non-decline symptoms is shown in Fig. 10. In 2020, when no heatwave occurred, *Q. frainetto* ecophysiological responses were similar for declining and non-

Preprints (www.preprints.org) | NOT PEER-REVIEWED | Posted: 29 July 2022 doi:10.20944/preprints202207.0440.v1

declining tree, suggesting that there was no evident sign of water stress in the summer of 2020. From Fig. 6, we see in fact that wdi is below 10 °C in July. In contrast, in 2021, not only the water vapour exchange is more than double, showing that the evapotranspiration has increased because of the larger difference $T_s - T_d$, when the declining trees behave differently with respect to the non-declining vegetation, showing that the non-declining trees are suffering from the water deficit much more than the healthy vegetation.

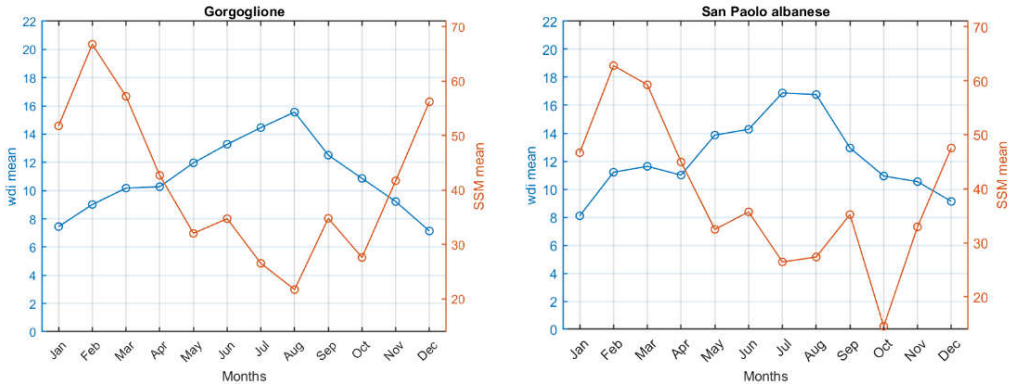

Figure 9. Monthly time series of ssm and wdi in 2017 for the two-tower stations of Gorgoglione (left) and S. Paolo Albanese (right).

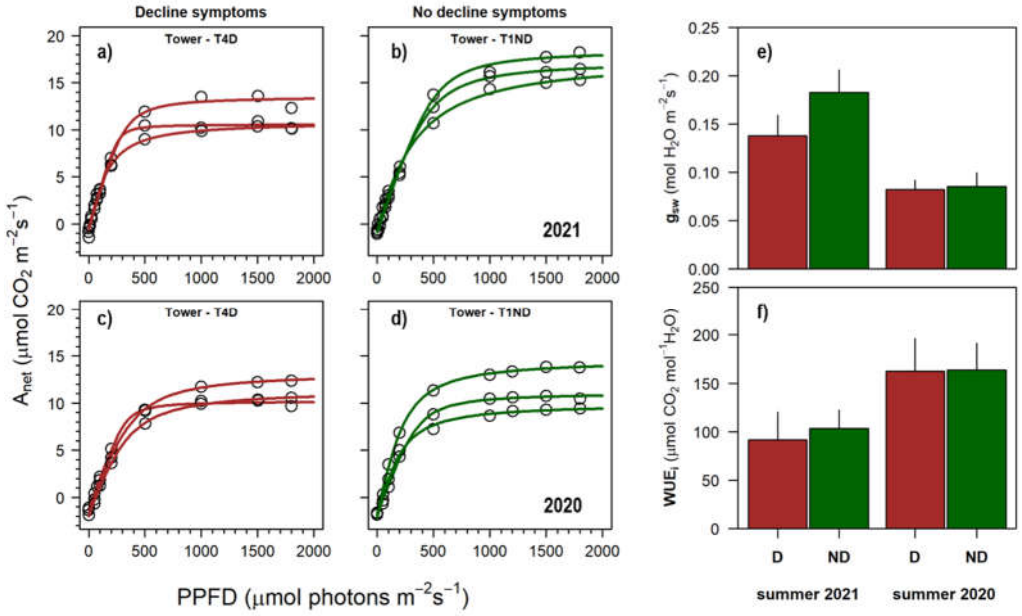

Figure 10. Ecophysiological responses of declining (D) and non-declining (ND) *Q. frainetto* trees of San Paolo Albanese forest stand site. In panels a),b),c) and d) net photosynthesis curve (An, µmolCO_2 m^{-2} s^{-1}) while in panels e) and f) average values of stomatal conductance (gsw, mmolH_2O m^{-2} s^{-1}) and intrinsic water use efficiency (WUEi, µmolCO_2 $mmol^{-1}$ H_2O) measured on summer 2020 and 2021. PPFD represents the photosynthetic photon flux density (µmol photons m^{-2} s^{-1}). The black vertical bar represents 1st deviation standard.

It is also interesting to note that for CO_2, flux exchange had an opposite behaviour to H_2O. In summer 2020, when there were good climatic conditions, we observed an exchange larger than in 2021. In 2021 the results showed that the vegetation was reducing photosynthesis activity because of stress conditions.

Preprints (www.preprints.org) | NOT PEER-REVIEWED | Posted: 29 July 2022 doi:10.20944/preprints202207.0440.v1

4. Discussion

In summer 2017, Southern Europe and the Euro-Mediterranean were hit by an exceptional heat wave [3,29]. After an outstanding warm June in western Europe, the heat returned to southern Italy in July. It contributed to more than 400 wildfires, which destroyed some 800 km² of forest and vegetated areas. The number of fires has been unprecedented in the last 20 years. Furthermore, early August saw a particularly intense heat wave described as the "worst heat wave since 2003", with the air temperature above 40 C in many parts of Italy.

In the quest for possible satellite indices to assess and possibly, mitigate the effect of long-lasting drought on vegetation, we have devised an index, ***wdi***, which takes advantage of the IASI capability to retrieve surface simultaneously with atmospheric parameters. The ***wdi*** index is meant to identify regions where particular weather conditions can produce water deficits. The index is not intended as an estimate or an estimator of evapotranspiration. This process is also affected by vegetation/crop characteristics, environmental conditions, and cultivation types. Therefore, there is too much variability, which cannot be condensed into a single index. The ***wdi*** parameter is a bulk index, which can help to monitor forest and wood regions suffering from long-lasting droughts because of adverse weather conditions. It can be mapped on a regional and even global scale, allowing us to monitor drought processes at a glance. The ***wdi*** maps could be important to monitor and evaluate the risk of fires in the large forested area, which is otherwise inaccessible. Also, we have shown that in regions where the vegetal ecosystem has a particular fragility to water deficit, the index can soon quantify the possible danger and require in situ more accurate observations.

In this respect, wdi is most effective in the case of a heatwave. In the wintertime, for example, large values of wdi could be linked to a dry atmosphere and low air temperature. In effect, this is the case in January 2017 for the more southern area on the map of Fig. 5, which belongs to the high mountains of the Sila chain. Also, in summer, very humid and warm conditions could lead to wdi~0. For example, this is the case of the coastal regions in July-August 2017, as seen again in the map in Fig. 5. For these cases, it is better to look separately at the map of T_s, and T_d. In this respect, we observe that the dew point temperature has been individuated as a key parameter to compute sophisticated indicators of health stress for human beings during heatwaves [30].

Some words of caution should also be said about the temporal sampling of ***wdi***. The occasional occurrence of a high ***wdi*** for one day should be of no concern. Drought is a process taking several days or months. The severity of the process depends on its time continuity and persistence. Therefore, it is crucial to assess the persistence of the process, which can be done by looking at time series. Averaging over several days can help to understand the persistence of the phenomenon. Another important point concerns the capability of the retrieval system to solve the daily cycle, which cannot be done with the present polar satellite IASI instrument. During the night, the surface temperature could go below the dew point temperature and cause water vapour to condense at the surface. Therefore it could be interesting to examine separately day and night. Hopefully, this could be the case when the MTG-IRS (https://www.eumetsat.int/mtg-infrared-sounder) is put in orbit.

5. Conclusions

Exploiting the capability of the IASI instrument to perform simultaneous retrievals of surface and thermodynamical parameters, we have developed an index called water deficit index or ***wdi***. The index is intended chiefly in the presence of evident droughts because it can assess the severe water deficit for vegetation and particular forests.

The tool has been exemplified in a target area in the South of Italy, suffering from an intense drought and heatwave in 2017. When the heatwave is developing, we have shown, with the help of correlative observations of surface soil moisture and leaf area index, that

wdi can assess how severe is the water deficit. Particularly interesting is the anti-correlation with the surface soil moisture. The soil water content and the ability of the soil to transport water to the roots govern the transpiration rate of vegetation. In case ***wdi*** becomes large, we have found that ***ssm*** gets smaller, which shows how ***wdi*** is capable of capturing processes occurring at the surface-atmosphere interface.

The possible usage of *wdi* includes monitoring the large forested area for the increased risks of wildfire and assessing mitigation measures for regions whose green ecosystems are in danger and more fragile because of climate change.

Author Contributions: Guido Masiello contributed to the overall conceptualization and organized the field campaigns; Francesco Ripullone revised the paper, contributed to funding acquisition, and organized the field campaigns; Italia De Feis developed the 2D-OI scheme; Angelo Rita was involved in the formal analysis of the field campaign data and contributed to the final editing; Luigi Saulino has contributed to the editing of the paper and was involved in the field campaigns; Pamela Pasquariello contributed to the analysis of IASI data; Angela Cersosimo contributed to the implementation of the 2D-OI scheme; Sara Venafra contributed to the software development and data acquisition; Carmine Serio wrote the paper, contributed to funding acquisition and conceptualization of the wdi index. All authors have read and agreed to the published version of the manuscript.

Funding:. The Italian Ministry of University has supported this research in the framework of the project ARS01_00405, "OT4CLIMA" (D.D. 2261 del 6.9.2018, PON R&I 2014-2020 and FSC).

Data Availability Statement: The IASI L1C data used in this study are directly available from EUMETSAT. They are received through the EUMETCast near real-time data distribution service.

Surface soil moisture data were downloaded from the site https://land.copernicus.eu/global/products/ssm

Leaf area index data were downloaded from the site https://land.copernicus.eu/global/products/lai

All L2 IASI data computed in the paper are available on request by the authors.

Data used to build up Fig. 10 are available on request by the authors.

Acknowledgments: IASI has been developed and built under the responsibility of the Centre National d'Etudes Spatiales (CNES, France). Instrumentation flies onboard the Metop satellites as part of the EUMETSAT Polar System.

Conflicts of Interest: The authors declare no conflict of interest.

References

1. Cramer, W. ; Guiot, J. ; Fader, M. ; *et al.* Climate change and interconnected risks to sustainable development in the Mediterranean. *Nature Clim Change,* ***2018,*** **8,** 972–980. https://doi.org/10.1038/s41558-018-0299-2
2. Adams, H.D.; Zeppel, M.J.B.; Anderegg, W.R.L.; *et al.* A multi-species synthesis of physiological mechanisms in drought-induced tree mortality. *Nat Ecol Evol*, ***2017,*** 1**,** 1285–1291 https://biblioproxy.cnr.it:2481/10.1038/s41559-017-0248-x
3. Rita, A; Camarero, JJ; Nolè, A; et al. The impact of drought spells on forests depends on site conditions: The case of 2017 summer heat wave in southern Europe. *Glob Change Biol*. **2020**; 26: 851– 863. https://doi.org/10.1111/gcb.14825
4. Vincente-Serrano, S.M.; Pons-Fernandez, X.; Cuadrat-Prats, J.M. Mapping soil moisture in the central Ebro river valley with Landsat and NOAA satellite imagery: a comparison with meteorological data. *International Journal of Remote Sensing* **2004**, 25 (20), 4325–4350.
5. Vicente-Serrano, S.M.; Cuadrat-Prats, J.M.; Romo, A. Aridity influence on vegetation patterns in the middle Ebro Valley (Spain): Evaluation by means of AVHRR images and climate interpolation techniques. *Journal of Arid Environments*, **2006**, 66 (2), 353–375.
6. Chen, S.; Wen, Z.; Jiang, H.; Zhao, Q.; Zhang, X.; Chen, Y. Temperature Vegetation Dryness Index Estimation of Soil Moisture under Different Tree Species. *Sustainability* **2015**, *7*, 11401-11417. https://doi.org/10.3390/su70911401
7. Masiello, G.; Cersosimo, A.; Mastro, P.; Serio, C.; Venafra, S.; Pasquariello, P. Emissivity-based vegetation indices to monitor deforestation and forest degradation in the Congo basin rainforest, *Proc. SPIE 11528, Remote Sensing for Agriculture, Ecosystems, and Hydrology* XXII, **(20 September 2020);** 115280L doi: 10.1117/12.2573488
8. Karnieli, A.; Agam, N.; Pinker, R.T.; Anderson, M.; Imhoff, M.L.; Gutman, G.G.; Panov, N.; and Goldberg, A. Use of NDVI and Land Surface Temperature for Drought Assessment: Merits and Limitations. **J. Climate**, **2010** 23, 618–633, https://doi.org/10.1175/2009JCLI2900.1

9. Hilton, F.; Armante, R.; August, T.; et al. Hyperspectral Earth Observation from IASI: Five Years of Accomplishments, *Bulletin of the American Meteorological Society*, **2012**, *93*(3), 347-370. Retrieved June 4, 2022, from https://journals.ametsoc.org/view/journals/bams/93/3/bams-d-11-00027_1.xml
10. Ru, C.; Hu, X.; Wang, W.; Ran, H.; Song, T.; Guo, Y. Evaluation of the Crop Water Stress Index as an Indicator for the Diagnosis of Grapevine Water Deficiency in Greenhouses. *Horticulturae* **2020**, *6*, 86. https://doi.org/10.3390/horticulturae6040086
11. Mishra, A.K.; Singh, V.P. A review of drought concepts. *J. Hydrol.* **2010**, *391*, 202–216.
12. Behrangi, A.; Loikith, P.C.; Fetzer, E.J.; Nguyen, H.M.; Granger, S.L. Utilizing Humidity and Temperature Data to Advance Monitoring and Prediction of Meteorological Drought. *Climate* **2015**, *3*, 999-1017. https://doi.org/10.3390/cli3040999
13. Francesco Ripullone, J Julio Camarero, Michele Colangelo, Jordi Voltas. Variation in the access to deep soil water pools explains tree-to-tree differences in drought-triggered dieback of Mediterranean oaks. *Tree Physiology*, (2020) 40(5), 591–604, https://doi.org/10.1093/treephys/tpaa026
14. Colangelo M, Camarero JJ, Borghetti M, Gentilesca T, Oliva J, Ripullone F, Redondo MA. Drought and Phytophthora are associated with the decline of oak species in southern Italy. *Front Plant Sci* (2018) 9:1595.
15. Bauer-Marschallinger, B. ; Freeman, V. ; Cao, S. ; Paulik, C. ; Schaufler, S. ; Stachl, T. ; Modanesi, S. ; Massari, C. ; Ciabatta, L. ; Brocca, L. ; Wagner, W. Toward Global Soil Moisture Monitoring With Sentinel-1: Harnessing Assets and Overcoming Obstacles. IEEE Transactions on Geoscience and Remote Sensing 2019, 1 - 20. DOI 10.1109/TGRS.2018.2858004
16. Fuster, B. ; Sánchez-Zapero, J. ; Camacho, F. ; García-Santos, V. ; Verger, A. ; Lacaze, R. ; Weiss, M. ; Baret, F. ; Smets, B. Quality Assessment of PROBA-V LAI, fAPAR and fCOVER Collection 300 m Products of Copernicus Global Land Service. Remote Sensing 2020, 12137, 1017. DOI 10.3390/rs12061017
17. Amato, U.; Masiello, G.; Serio, C.; and Viggiano, M. The σ-IASI code for the calculation of infrared atmospheric radiance and its derivatives," *Environmental Modelling & Software* **2002**, 17(7), 651–667.
18. Carissimo, A.; De Feis, I.; and Serio, C. The physical retrieval methodology for IASI: the δ-IASI code, *Environmental Modelling & Software* , **2005**, 20(9), 1111–1126.
19. Liuzzi, G.; Masiello, G.; Serio, C.; Venafra, S.; Camy-Peyret, C. Physical inversion of the full IASI spectra: Assessment of atmospheric parameters retrievals, consistency of spectroscopy and forward modelling, *Journal of Quantitative Spectroscopy and Radiative Transfer*, **2016**, 128-157, https://doi.org/10.1016/j.jqsrt.2016.05.022.
20. Serio, C.; Masiello, G.; and Liuzzi, G. Demonstration of random projections applied to the retrieval problem of geophysical parameters from hyperspectral infrared observations, *Appl. Opt.* **2016,** 55, 6576-6587, https://doi.org/10.1364/AO.55.006576
21. Rodgers, C.D. *Inverse Methods for Atmospheric Sounding: Theory and Practice*; World Scientific: Singapore, 2000.
22. Masiello, G.; Serio, C.; Venafra, S.; DeFeis, I.; and Borbas, E. E., Diurnal variation in Sahara desert sand emissivity during the dry season from IASI observations, *J. Geophys. Res. Atmos.*, **2014**, 119, 1626– 1638, doi:10.1002/jgrd.50863.
23. Masiello, G.; Serio, C.; Venafra, S.; Liuzzi, G.; Poutier, L.; Göttsche, F.-M. Physical Retrieval of Land Surface Emissivity Spectra from Hyper-Spectral Infrared Observations and Validation with In Situ Measurements. *Remote Sens.* **2018**, *10*, 976. https://doi.org/10.3390/rs10060976
24. Masiello, G.; Serio, C.; Deleporte, T.; Herbin, H.; Di Girolamo, P.; Champollion, C.; Behrendt, A.; Bosser, P.; Bock, O.; Wulfmeyer, V.; Pommier, M.; Flamant, C. Comparison of IASI water vapour products over complex terrain with COPS campaign data *Meteorologische Zeitschrift*, **2013,** Vol. 22 No. 4, 471 – 487, doi: 10.1127/0941-2948/2013/0430
25. Huang, J. A Simple Accurate Formula for Calculating Saturation Vapor Pressure of Water and Ice, *Journal of Applied Meteorology and Climatology*, **(2018)** *57*(6), 1265-1272. Retrieved Jun 14, 2022, from https://journals.ametsoc.org/view/journals/apme/57/6/jamc-d-17-0334.1.xml
26. Sonntag, D. Important new values of the physical constants of 1986, vapour pressure formulations based on the ITS-90, and psychrometer formulae. *Zeitschrift für Meteorologie*, (**1990**) *40*(5), 340-344.
27. Allen, R.G.; Pereira, L.S.; Raes, D.; Smith, M. *Crop evapotranspiration - Guidelines for computing crop water requirements - FAO Irrigation and drainage paper 56,* FAO-Food and Agriculture Organization of the United Nations, Rome, Italy, **1998**, Retrieved June 4, 2022, from https://www.fao.org/3/x0490e/x0490e00.htm
28. De Feis, I.; Masiello, G.; Cersosimo, A. Optimal Interpolation for Infrared Products from Hyperspectral Satellite Imagers and Sounders. Sensors 2020, 20, 2352. https://doi.org/10.3390/s20082352
29. Kew, S. f.; Philip, S. Y.; Jan van Oldenborgh, G.; van der Schrier, G.; Otto, F. E. L.; Vautard, R. The Exceptional Summer Heat Wave in Southern Europe 2017, Bulletin of the American Meteorological Society, (**2019**)., 100(1), S49-S53. Retrieved Jun 26, 2022, from https://journals.ametsoc.org/view/journals/bams/100/1/bams-d-18-0109.1.xml
30. Lee, S.-Y.; Lung, S.-C.C.; Chiu, P.-G.; Wang, W.-C.; Tsai, I.-C.; Lin, T.-H. Northern Hemisphere Urban Heat Stress and Associated Labor Hour Hazard from ERA5 Reanalysis. Int. J. Environ. Res. Public Health 2022, 19, 8163. https://doi.org/10.3390/ijerph19138163